2016 Spring Technical Meeting
Eastern States Section of the Combustion Institute
Hosted by Princeton University
March 13-16, 2016

# Effects of fuel structure on soot precursors in a laminar co-flow flame

*A. Makwana*[1], *A. Jain*[1], *M. Linevsky*[1], *S. Iyer*[1], *R. Santoro*[1], *T. Litzinger*[1], *Y. Xuan*[1], *J. O'Connor*[1]

[1]*Mechanical and Nuclear Engineering, Pennsylvania State University, University Park, PA, USA*

The goal of this work is to aid in understanding the effects of fuel molecular structure on the spatial development of polycyclic aromatic hydrocarbons (PAH), or soot precursors, in an axisymmetric, co-flow, laminar flame configuration at atmospheric pressure. Two fuels with varying molecular structure are investigated: iso-octane/n-dodecane mixture and m-xylene/n-dodecane mixture. The flames investigated are non-premixed and rich premixed (jet equivalence ratio of 6) flames, and the total carbon flow rate is kept constant to facilitate comparison between fuels. A laser-induced fluorescence technique is used to obtain spatially-resolved PAH in the jet flames. The PAH are identified into two classes: single/two ring aromatics (small) and molecules having three/four rings (large). The experimental results indicate that the level of aromatics for m-xylene/n-dodecane fuel is higher compared to iso-octane/n-dodecane fuel. The comparison of PAH in non-premixed and premixed flames show significant differences in the spatial development of PAH along the downstream direction. These results are compared to initial simulation results and a methodology for using the PAH-LIF technique for validating soot models in laminar jet flames is proposed.

## 1. Introduction

Scarce energy resources, stricter environmental requirements, worldwide air traffic growth, and rising fuel prices all lead to an increasing interest in alternative jet fuels. Alternative jet fuels derived from micro-organisms, pyrolysis oil, and alcohols [1] have unusual molecular distribution relative to the current approved fuels. The gas phase kinetics and hence, the combustion behavior, is affected by the fuel composition [2]. This necessitates the need to understand the chemical and physical effects of fuel molecular structure on the combustion behavior. The work in this paper is a part of collaborative efforts between multiple experimental and computational groups to extend the fundamental understanding of chemical effects of fuel molecular structure on emissions, particularly soot. The soot formation process has been studied in many flame configurations, which include diffusion flames [3, 4], premixed flames [5, 6], opposed jet flames [7, 8], turbulent flames [9], spray flames [9], and diesel engines [10]. A number of studies have focused on understanding the effect of molecular structure on emissions [11-14]. The present study aims to advance the current understanding of effect of molecular structure on soot and its precursors.

Polycyclic aromatic hydrocarbons (PAH) are understood to be the precursors of soot [15-17]. However, the steps to form of the first nascent soot particle from the gas phase are still not clear. A better understanding of soot formation in jet flames can be gained by characterizing the development of PAH. The PAH measurements obtained from jet flames can be used to validate and improve the soot models, as has been started in the current work.

## 2. Methods/Experimental

### *2.1 Burner and Burner system*

A co-annular laminar flame burner is used to study soot formation in a well-characterized, steady, laminar flame. This burner is similar to the co-annular laminar flame burner used by Santoro *et al*. [3]. The burner consists of two concentric brass tubes. The inner fuel tube diameter is 11.1 mm. This tube protrudes 4 mm above the plane of the co-flow. The outer air tube has a 101.6 mm diameter, and the air flow passes through a dense honeycomb to provide a well-characterized boundary condition for the fuel jet. The heat for fuel vaporization is provided by heating tapes that are wrapped around the tubing system, and nitrogen is used as a carrier gas for the fuel. The temperature of the heating tapes is maintained at 250$^{o}$ C in order to vaporize the fuel. Gas chromatography has been used on the fuel-air-nitrogen mixture at the exit of burner tube to ensure that no fuel pyrolysis has occurred in the tubing system. A detailed description of the burner and the burner system is discussed in Makwana *et al*. [18].

### *2.2 Diagnostic method*

In the present study, planar laser induced fluorescence (PLIF) is used to obtain measurement of aromatic hydrocarbons in the jet flames. The PAH molecules exhibit broadband fluorescence over a wide range of excitation wavelengths [19, 20]. The study by Zizak *et al*. [21] reported that PAH fluoresce wavelength is dependent on the size of the PAH molecule. The fluorescence wavelength shifts to longer wavelength as the molecule size increases. This property is used in the present study to identify two different classes of PAHs: one and two ring aromatics, and molecules having more than two rings. Two sets of wavelength filters are used in front of an ICCD camera to capture the fluorescence for each molecule class. A combination of WG320 and UG11 filters transmit fluorescence in the range from 320 nm to 380 nm, which corresponds to the "small" aromatics. A combination of GG420 and BG12 filters transmit fluorescence in the range from 420 nm to 480 nm, which corresponds to the "large" aromatics. The LIF experiment is shown in Figure 1.

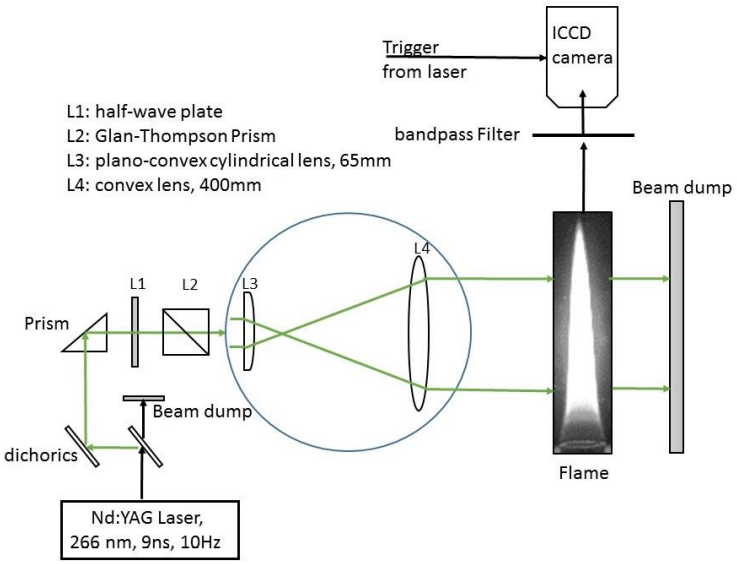


**Figure 1: Optical setup for laser induced fluorescence.**

A 1 mJ laser pulse energy is used to create a 48 mm laser sheet; the laser intensity is below the threshold for generating LII signals. The camera is gated for 170 ns within the laser pulse. A total of 250 images are collected for each flame condition to improve the signal to noise ratio.

*2.3 Experimental Conditions*

The fuel test matrix is comprised of binary mixtures of a normal paraffin, n-dodecane, with an iso-paraffin (iso-octane), and an aromatic specie (m-xylene). This initial study uses two fuel structures that represent two of the four molecular classes found in a real aviation fuel. The two blending species are selected to have a similar boiling point. The binary mixture of 75% n-dodecane and 25% m-xylene by volume fraction is the base fuel. All binary mixtures are chosen such that the carbon fraction of the mixture is the same as the baseline fuel. The mixture properties are presented in Table 1.

| Name | Component | Volume fraction (%) | Boiling point (℃) | Mass fraction (%) | Hydrogen content (%) | H/C ratio | Jet Equivalence ratio ($\phi$) |
|---|---|---|---|---|---|---|---|
| m-X | m-xylene | 25 | 139 | 27.7 | 13.8 | 1.9 | Inf (non-premixed) and 6 |
| | n-dodecane | 75 | 216 | 72.3 | | | |
| i-$C_8$ | iso-octane | 30.6 | 99 | 28.9 | 15.5 | 2.19 | |
| | n-dodecane | 69.4 | 216 | 71.1 | | | |

**Table 1: Fuel Matrix.**

*2.4 Model description*

The flow solver used in this work is the NGA code [22]. The NGA solver uses staggered variables and allows for accurate, robust, and flexible simulations of both laminar and turbulent reactive flows in complex geometries. This framework has been applied in a wide range of test problems, including laminar and turbulent flows, constant and variable density flows, as well as Large-Eddy Simulations (LES) and Direct Numerical Simulations (DNS) [23]. The species mass fractions and temperature are transported using the BQUICK scheme, which ensures that the physical bounds of appropriate quantities are numerically preserved throughout the simulation without adding significant artificial diffusion [24]. A recently-developed computationally-efficient, semi-implicit, iterative method is used for the time-integration of chemical source terms for the transport equations of gas-phase species. This method has been shown to be free of lagging errors, as efficient as an explicit time-integration per time step, and capable of using large, stable time-step sizes [25]. These numerical methods guarantee globally second-order accuracy in both space and time [25].

The detailed chemistry model employed in the current work is taken from Ref. [26]. It contains 185 species and 1903 reactions (forward and backward reactions counted separately) and takes into account all major pathways of PAH formation. This chemical model has been extensively tested and validated in multiple configurations, including laminar premixed flames, laminar diffusion flames, and homogeneous reactors. The soot model employed in the current study is taken from Ref. [27]. Soot particles are described as fractal aggregates using a bi-variate approach based on the total volume and total surface area. The population of the soot particles is statistically

described using a bi-variate soot Number Density Function (NDF), and is approximated by two delta functions, following previous work [27].

## 3. Results and Discussion

The LIF signal captured by the camera can be related to the number density of the specie if the local temperature, fluorescence yield, collection efficiency of camera, and camera response function are known [28]. In the present study, the LIF of small and large aromatics is collected from a number of different species and quenching effects for all the aromatics are not well characterized. As a result, semi-quantitative comparison is presented in this paper. In order to compare the simulation results with the experiment results, the mole fraction of aromatics species obtained from the simulation is converted to mole concentration, assuming ideal gas. The mole fraction of each species is multiplied by the corresponding fluorescence cross sections to obtain the "computational LIF signal." The fluorescence cross sections [29, 30] along with the corresponding aromatic species are listed in Appendix A. The LIF counts from experiment have been corrected for the non-uniform laser sheet energy, background, and dark signal. The background image is obtained under the same experimental parameters as the LIF experiment without a laser, and this image is subtracted from the LIF image.

### *3.1 Effect of fuel structure on small and large aromatics.*

Figure 2 shows the comparison of the two-dimensional LIF signals obtained for small and large aromatics for the n-dodecane/m-xylene flame. In all figures of this kind, part (a) is a reference image taken using a Canon A640 camera to indicate flame height. Parts (b) and (c) show the profiles of the small rings from experiment and simulation, respectively. Similarly, parts (d) and (e) show the profiles of the large rings from experiment and simulation, respectively.

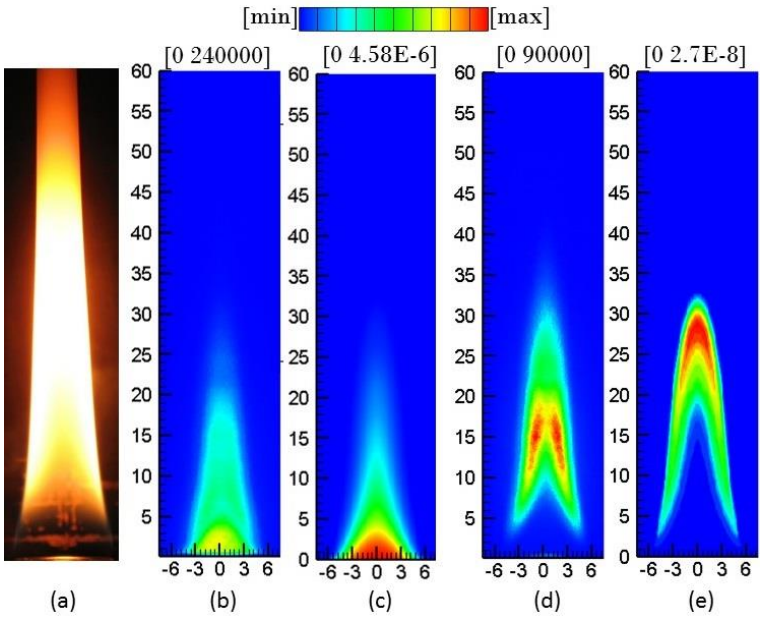


**Figure 2: Two-dimensional LIF signals obtained for mX- ϕ=Inf-0.2N2 flame (a) visible flame image; (b) small aromatics from experiment; (c) small aromatics from simulation; (d) large aromatics from experiment; (e) large aromatics from simulation.**

Figure 2(b) shows that the small aromatics are present at the tube exit because m-xylene itself is a one-ring aromatic and fluoresces in the 320-380 nm bandwidth. The small aromatics initially show a trend of rapid decrease in concentration and then continue to decrease at steady rate along the downstream direction. The initial rapid decrease in concentration is due to the consumption of m-xylene. The fall-off rate is tempered as other small aromatics are formed. The small aromatics concentration decreases as the process of conversion to large aromatics dominates over the production as seen in Figure 2(d). The large aromatics initially appear at 3-4 mm height above the burner (HAB) in the annular region of the flame and then appear along the centerline at 5-6 mm HAB. Along the centerline, the large aromatics concentration does not reach the levels that occur in the annular region. The concentration of large aromatics decreases as they are converted to soot or oxidized. The trend of conversion of fuel to one or two ring aromatics, then to larger three-four aromatics and eventually soot agrees with the previous findings of soot formation in flames [15, 17, 31].

Figure 2(c) shows that the simulation captures the spatial development of the small aromatics as observed in the experiment. The large aromatics from simulation, in Figure 2(e), demonstrate that the peak in the large aromatics occurs on the centerline at 25-30 mm HAB compared to the experiment results, which shows a peak in the annular region at 15-20 mm HAB. Figure 3 shows the comparison of the development of the small and large aromatics along the flame centerline. The small aromatics in the simulation follow the profile of the small aromatics observed in the experiment. However, the first appearance of the large aromatics along the centerline is delayed in the simulation as compared to the experiment. In the simulation, the large aromatics appear at 18 mm HAB, while in experiment, they are first observed at 5 mm HAB. Large aromatics first appear in the annular region at 3-4 mm HAB in both the simulation and the experiment.

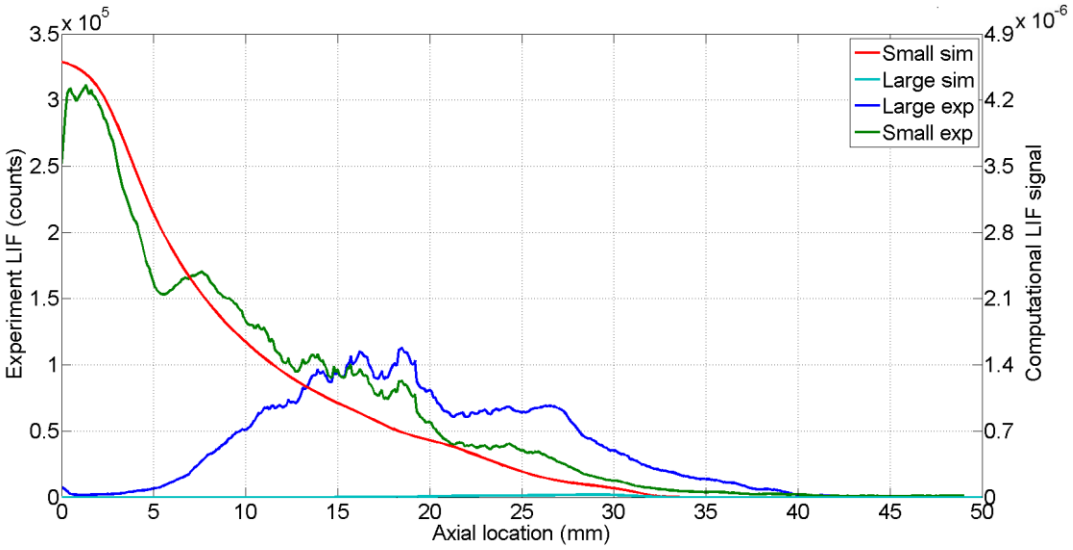


**Figure 3: Axial comparison of small and large aromatics between simulation and experiment mX- ϕ=Inf-0.2N2.**

Figure 4 shows the two-dimensional LIF signals obtained for small and large aromatics for a non-premixed n-dodecane/iso-octane flame. Figure 4(b) shows that the small aromatics start to appear first in the annular region of the flame at 3 mm HAB. At locations farther downstream, the concentration of aromatics in the annular region decreases due to their conversion to the large

aromatics, as can also be seen in Figure 4(d). The large aromatics start to appear at 5-6 mm HAB. The central region has no small aromatics near the base, but the concentration of small aromatics starts to increase at 5 mm HAB, peaking and then decreasing at 16-17 mm HAB due to conversion to the large aromatics. Figure 4(d) shows that the spatial development of the large aromatics for a non-premixed iso-octane/n-dodecane flame is similar to the non-premixed m-xylene flame in Figure 2(d). The large aromatic concentration is higher in m-xylene mixture as compared to the iso-octane flame. This is because m-xylene already has a single ring, and hence, the formation of larger aromatics is accelerated.

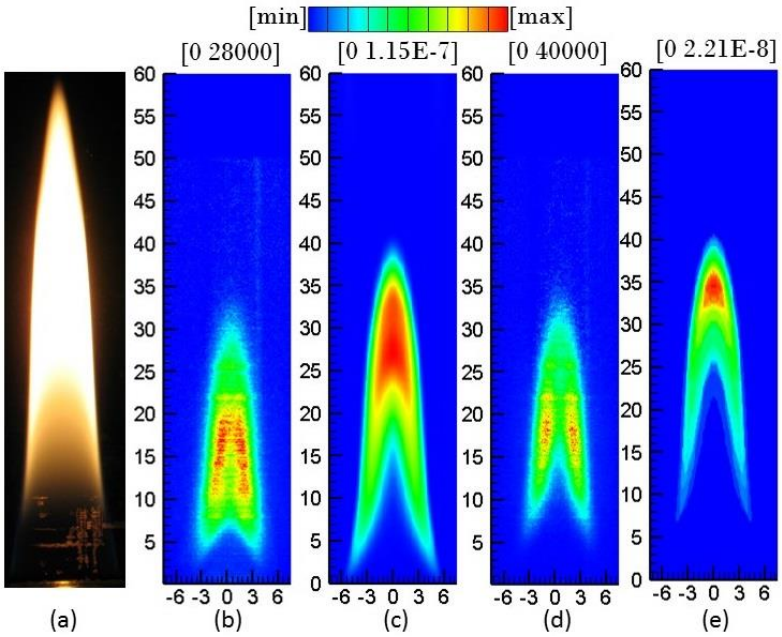


**Figure 4: Two-dimensional LIF signals obtained for iC8- ϕ=Inf-0.2N2 flame (a) visible flame image; (b) small aromatics from experiment; (c) small aromatics from simulation; (d) large aromatics from experiment; (e) large aromatics from simulation.**

The simulation results for n-dodecane/iso-octane fuel show similar trends as the experimental results, as observed in n-dodecane/m-xylene fuel. Figure 4 (c) and (e) indicate that the peak in the small and large aromatics occur in the centerline, while in experiment they occur in the annular region. The annular region shows the first appearance of the small and large aromatics at 3-4 mm HAB and 6-7 mm HAB, respectively, in both the simulation and the experiment.

Figure 5 shows the comparison of the development of the small and large aromatics along the flame centerline in the simulation and the experiment. The small aromatics start to increase at 5 mm HAB in the experiment and simulation. However, the rate of increase of the small aromatics is higher in the experiment as compared to the simulation. As a result, the small aromatics peak at 17 mm HAB in the experiment results while it peaks at 26 mm HAB in the simulation result. The formation of the large aromatics is also delayed along the flame centerline in the simulation compared to in the experiment. In the simulation, they start to increase at 20 mm HAB, whereas in experiment, large aromatics start to increase at 5 mm HAB.

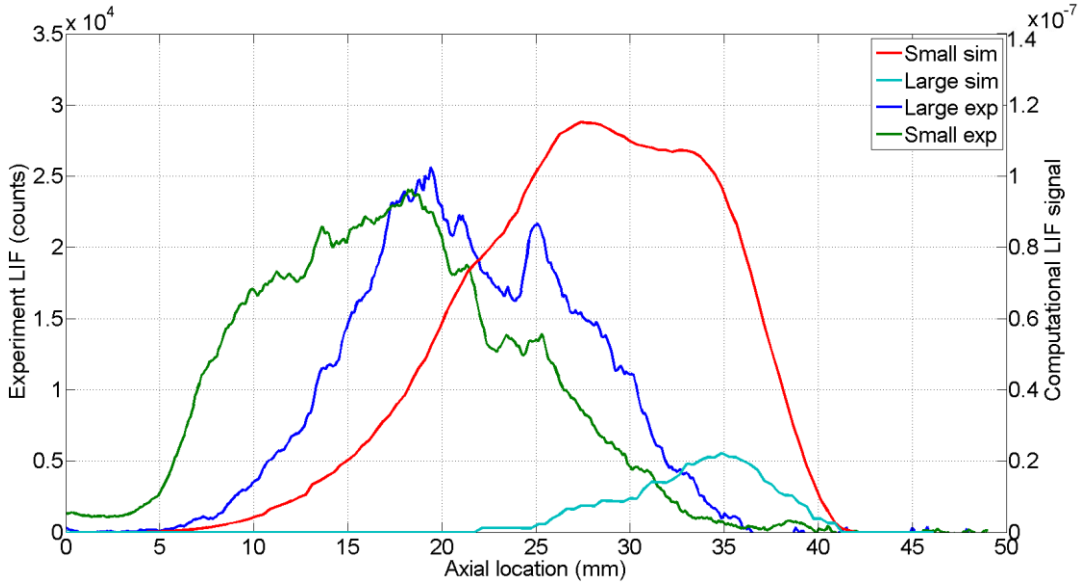


**Figure 5: Axial comparison of small and large aromatics between simulation and experiment iC8- ϕ=Inf-0.2N2.**

One reason for this delay in aromatic formation may be differences in temperature. Figure 6 shows the comparison of the axial temperature profile from the experiment and the simulation for both n-dodecane/iso-octane and n-dodecane/m-xylene fuel mixtures. The temperature is measured using an R-type thermocouple and is radiation corrected [18]. The agreement between simulation and experiment results is good, considering the temperature measurement uncertainty of ±100 K.

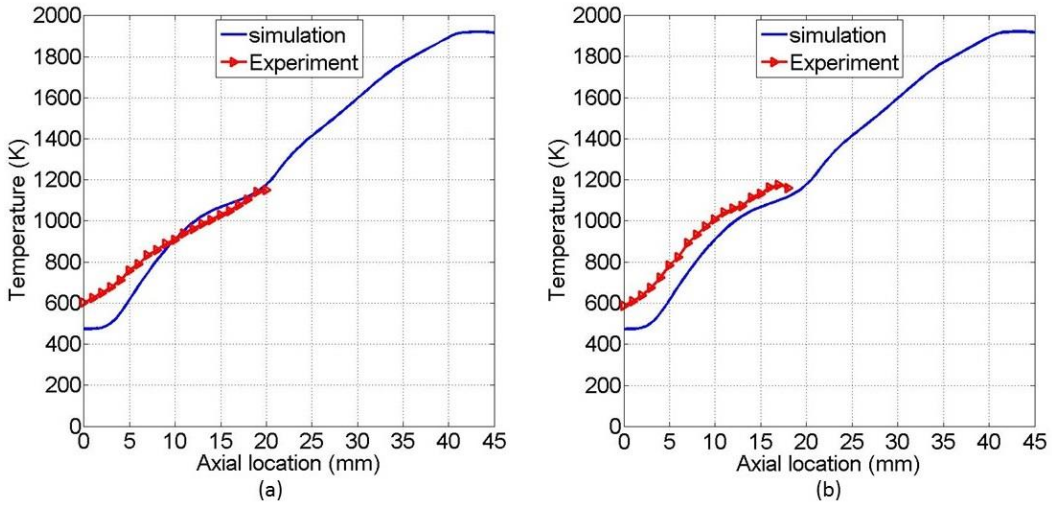


**Figure 6: Axial temperature comparison between the simulation and the experiment (a) iC8- ϕ=Inf-0.2N2; (b) mX- ϕ=Inf-0.2N2.**

*3.2 Effect of air addition on small and large aromatics*

Figure 7 shows the two-dimensional LIF signals obtained for small and large aromatics for a non-premixed and rich-premixed (ϕ=6) n-dodecane/iso-octane flame. The comparison shows how the spatial development of aromatics changes when air is premixed with fuel. First, in the non-premixed flame, shown in Figure 7(b) and (c), the peak in the small and large aromatics occurs in

the annular region. However, for the rich premixed flame, shown in Figure 7(e) and (f), the peak of both the small and large aromatics occurs on the flame centerline. Additionally, the formation of the small and large aromatics is delayed along the centerline in the rich premixed flame. Finally, the level of small and large aromatics in the premixed flame is less compared to the non-premixed flame. This reduction in aromatic concentration is the result of two effects. First, the premixing causes the carbon in the fuel to oxidized more quickly and hence, less carbon is available for the ring formation. Second, the LIF signals are quenched due to the presence of oxygen.

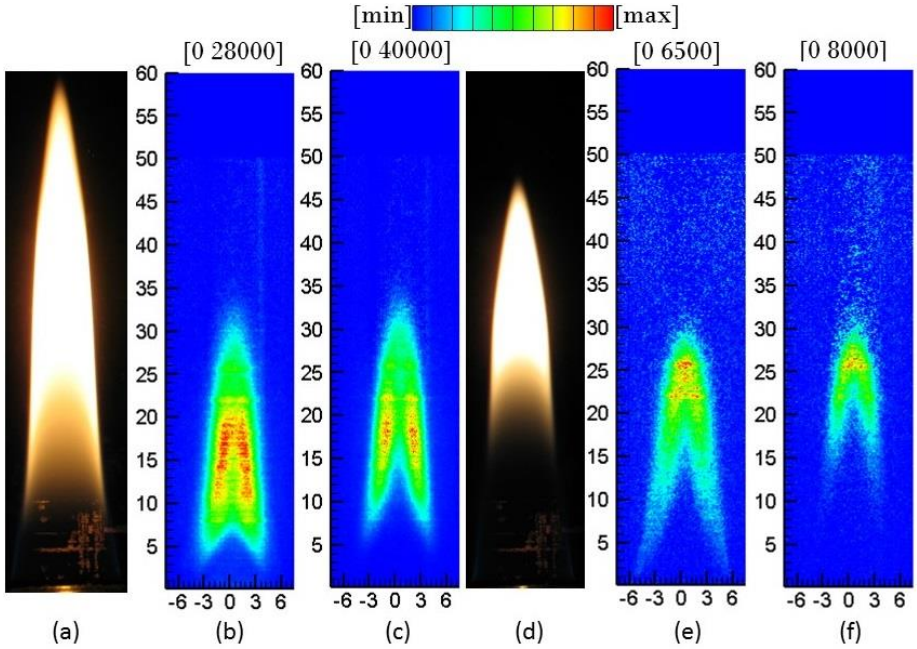


**Figure 7: Two-dimensional LIF signals obtained for (a) visible flame image iC8-ϕ=Inf-0.2N2; (b) small aromatics iC8-ϕ=Inf-0.2N2; (c) large aromatics iC8-ϕ=Inf-0.2N2; (d) visible flame image iC8-ϕ=6-0.2N2; (e) small aromatics iC8-ϕ=6-0.2N2; (f) large aromatics iC8- ϕ=6-0.2N2.**

## 4. Conclusions and Future Work

Qualitative broadband PLIF measurements for two classes of aromatics are obtained for a paraffin (n-dodecane/iso-octane) and an aromatic fuel (n-dodecane/m-xylene). The concentration of the small aromatics for the m-xylene fuel is higher in magnitude and spatially different compared to the corresponding iso-octane flame. In the m-xylene flame, presence of one ring aromatic accelerates the formation of the two-ring aromatics and PAHs. The large aromatics for the m-xylene fuel shows spatial development similar to the iso-octane flame. The PLIF measurements obtained for the iso-octane flame shows that the peak in the small and large aromatics occur in the annular region for the non-premixed flame, while for the premixed flame it occurs on the flame centerline. These initial tests indicate that this PLIF technique can provide valuable information about the development of PAH and soot in jet flames, and will be applied to other fuels in the future. The simulation framework is unable to capture all of the spatial behavior of the large aromatics correctly. It also shows a delayed onset of small and large aromatics for the iso-octane flame. To address these issues, capabilities are being added to the NGA code to better describe the oxidation behavior of soot. Efforts are also underway to identify the smoking nature of heavily sooting flames.

## Acknowledgements

The authors also wish to acknowledge the support of this work provided by the Strategic Environmental Research and Development Program (WP-2145) under the direction of Dr. Robin Nissan and Mr. Bruce Sartwell.

## References

1. Edwards, T., C. Moses, and F. Dryer. *Evaluation of combustion performance of alternative aviation fuels*. in *Nashville, 46th AIAA/ASME/SAE/ASEE Joint Propulsion Conference & Exhibit, AIAA-2010-7155*. 2010.
2. Colket, M., T. Edwards, S. Williams, N.P. Cernansky, D.L. Miller, F. Egolfopoulos, P. Lindstedt, K. Seshadri, F.L. Dryer, and C.K. Law. *Development of an experimental database and kinetic models for surrogate jet fuels*. in *45th AIAA Aerospace Sciences Meeting and Exhibit*. 2007.
3. Santoro, R., H. Semerjian, and R. Dobbins, *Soot particle measurements in diffusion flames.* Combustion and Flame, 1983. **51**: p. 203-218.
4. Santoro, R., T. Yeh, J. Horvath, and H. Semerjian, *The transport and growth of soot particles in laminar diffusion flames.* Combustion Science and Technology, 1987. **53**(2-3): p. 89-115.
5. McEnally, C.S. and L.D. Pfefferle, *Experimental study of nonfuel hydrocarbons and soot in coflowing partially premixed ethylene/air flames.* Combustion and Flame, 2000. **121**(4): p. 575-592.
6. Bennett, B.A.V., C.S. McEnally, L.D. Pfefferle, and M.D. Smooke, *Computational and experimental study of axisymmetric coflow partially premixed methane/air flames.* Combustion and Flame, 2000. **123**(4): p. 522-546.
7. Joo, P.H., Y. Wang, A. Raj, and S.H. Chung, *Sooting limit in counterflow diffusion flames of ethylene/propane fuels and implication to threshold soot index.* Proceedings of the Combustion Institute, 2013. **34**(1): p. 1803-1809.
8. Wang, Y. and S.H. Chung, *Effect of strain rate on sooting limits in counterflow diffusion flames of gaseous hydrocarbon fuels: Sooting temperature index and sooting sensitivity index.* Combustion and Flame, 2014. **161**(5): p. 1224-1234.
9. Svensson, K.I., *Effects of fuel molecular structure and composition on soot formation in direct-injection spray flames.* 2005.
10. Nehmer, D.A. and R.D. Reitz, *Measurement of the effect of injection rate and split injections on diesel engine soot and NOx emissions*. 1994, SAE Technical Paper.
11. Kashif, M., P. Guibert, J. Bonnety, and G. Legros, *Sooting tendencies of primary reference fuels in atmospheric laminar diffusion flames burning into vitiated air.* Combustion and Flame, 2014. **161**(6): p. 1575-1586.
12. Kashif, M., J. Bonnety, A. Matynia, P. Da Costa, and G. Legros, *Sooting propensities of some gasoline surrogate fuels: Combined effects of fuel blending and air vitiation.* Combustion and Flame, 2015. **162**(5): p. 1840-1847.
13. Zhou, L., N. Dam, M. Boot, and L. de Goey, *Investigation of the effect of molecular structure on sooting tendency in laminar diffusion flames at elevated pressure.* Combustion and Flame, 2014. **161**(10): p. 2669-2677.
14. Mouis, A., A. Menon, V. Katta, T. Litzinger, M. Linevsky, R. Santoro, S. Zeppieri, M. Colket, and W. Roquemore, *Effects of m-xylene on aromatics and soot in laminar, N 2-diluted ethylene co-flow diffusion flames from 1 to 5atm.* Combustion and Flame, 2012. **159**(10): p. 3168-3178.
15. Frenklach, M. and H. Wang. *Detailed modeling of soot particle nucleation and growth*. in *Symposium (International) on Combustion*. 1991. Elsevier.
16. Frenklach, M., *Reaction mechanism of soot formation in flames.* Physical Chemistry Chemical Physics, 2002. **4**(11): p. 2028-2037.
17. D'Alessio, A., A. D'Anna, A. D'orsi, P. Minutolo, R. Barbella, and A. Ciajolo. *Precursor formation and soot inception in premixed ethylene flames*. in *Symposium (International) on Combustion*. 1992. Elsevier.
18. Makwana, A., Y. Wang, M. Linevsky, S. Iyer, R. Santoro, T. Litzinger, and J. O'Connor, *Capturing Soot Formation with the Use of Iso-Octane as a Surrogate for Fischer-Tropsch Fuel.* 9th U.S. National Combustion Meeting, May 17-20, 2015.

19. Prado, G., A. Garo, A. Ko, and A. Sarofim. *Polycyclic aromatic hydrocarbons formation and destruction in a laminar diffusion flame*. in *Symposium (international) on combustion*. 1985. Elsevier.
20. Beretta, F., A. D'Alessio, A. D'Orsi, and P. Minutolo, *UV and visible laser excited fluorescence from rich premixed and diffusion flames.* Combustion science and technology, 1992. **85**(1-6): p. 455-470.
21. Zizak, G., F. Cignoli, G. Montas, S. Benecchi, and R. Donde, *Detection of aromatic hydrocarbons in the exhaust gases of a gasoline ic engine by laser-induced fluorescence technique.* Rec. Res. Dev. Appl. Spectrosc, 1996. **1**: p. 17-24.
22. Desjardins, O., G. Blanquart, G. Balarac, and H. Pitsch, *High order conservative finite difference scheme for variable density low Mach number turbulent flows.* Journal of Computational Physics, 2008. **227**(15): p. 7125-7159.
23. Xuan, Y., *Progress in numerical modeling of non-premixed combustion*. 2014, California Institute of Technology.
24. Herrmann, M., G. Blanquart, and V. Raman, *Flux corrected finite volume scheme for preserving scalar boundedness in reacting large-eddy simulations.* AIAA journal, 2006. **44**(12): p. 2879-2886.
25. Savard, B., Y. Xuan, B. Bobbitt, and G. Blanquart, *A computationally-efficient, semi-implicit, iterative method for the time-integration of reacting flows with stiff chemistry.* Journal of Computational Physics, 2015. **295**: p. 740-769.
26. Xuan, Y. and G. Blanquart, *Numerical modeling of sooting tendencies in a laminar co-flow diffusion flame.* Combustion and Flame, 2013. **160**(9): p. 1657-1666.
27. Y. Xuan, G.B., *Two-dimensional flow effects on soot formation in laminar premixed flames.* Combustion and Flame, in press.
28. Hanson, R.K., J.M. Seitzman, and P.H. Paul, *Planar laser-fluorescence imaging of combustion gases.* Applied Physics B, 1990. **50**(6): p. 441-454.
29. Petarca, L. and F. Marconi, *Fluorescence spectra and polycyclic aromatic species in a n-heptane diffusion flame.* Combustion and flame, 1989. **78**(3): p. 308-325.
30. Suto, M., X. Wang, J. Shan, and L. Lee, *Quantitative photoabsorption and fluorescence spectroscopy of benzene, naphthalene, and some derivatives at 106–295 nm.* Journal of Quantitative Spectroscopy and Radiative Transfer, 1992. **48**(1): p. 79-89.
31. Richter, H. and J.B. Howard, *Formation of polycyclic aromatic hydrocarbons and their growth to soot—a review of chemical reaction pathways.* Progress in Energy and Combustion science, 2000. **26**(4): p. 565-608.

# Appendix A

| Species | Normalized quantum efficiency |
|---|---|
| A1, A1O, A1OH ,A1CH3 , A1CH2, A1CHO, A1CH2O, OA1CH3, A1C2H, A1C2H5, A1C2H4, A1C2H3, A1C2H2, A1CH3CH3, A1CH3CH2, A1CH3CHO, A1CHOCH2, A1CHOCHO. | 0.07 |
| A2, A2O, A2OH, A2CH2, A2CH3, A2CH2O, A2R5, A2R5C2H. | 1 |
| A3, A3R5 | 1.6 |
| A4, A4R5, FLTN | 2.4 |
| P2 | 0.3 |